Theoretical Studies of Hydrogen Abstraction from 2-Propanol by OH Radical

Ning Luo, David C. Kombo,† and Roman Osman*

Department of Physiology and Biophysics, Mount Sinai School of Medicine of the City University of New York, One Gustave L. Levy Place, New York, New York 10029

Received: July 8, 1996; In Final Form: November 13, 1996[⊗]

Hydrogen abstraction from 2-propanol by hydroxyl radical was investigated with *ab initio* quantum chemical methods at the level of MP2/6-31G*, with scaling of correlation energy. Both the geometries and the energetics of reactants, products, and transition state structures change significantly when electron correlation is included in the optimization process. An exhaustive search produced 16 transition state structures for the abstraction of the three distinct hydrogens in 2-propanol. Abstraction of the α-hydrogen has two distinct transition structures with very low barriers. The calculated rate constant for H_α-abstraction is close to that predicted by collision theory. Abstraction of the β-hydrogen has 11 different transition structures that can be classified into three groups on the basis of the presence or absence of hydrogen bonding between the OH radical and the hydroxy group of 2-propanol. The calculated rate constants for the individual pathways show that the non-hydrogen-bonded pathways contribute most of the flux for this process. There are three nearly degenerate transition structures in the abstraction of the hydroxyl hydrogen. The calculated rate constants for the combined ($H_\alpha + H_o$) and H_β-abstractions, respectively, are in good agreement with available experimental data. The kinetic isotope effect (KIE) for H_β-abstraction agrees very well with experimental data. The calculated KIE for ($H_\alpha + H_o$) abstraction shows a stronger temperature dependence than the experimental KIE. However, the weak temperature dependence supports the notion that H_α-abstraction may be collision controlled.

Introduction

Hydrogen abstraction from organic molecules by hydroxyl radical is an important reaction that takes place in many chemical processes. A wealth of experimental data has been accumulated on the rate constants for this type of reaction,[1] and a number of theoretical studies on the interactions of OH radical with various compounds have been published.[2−12] In addition to its general importance, hydrogen abstraction by OH radical is also one of the major initial steps in the process of radiation damage of DNA. Strand breaks may lead to a wide range of biological consequences including mutation and cell death.[13] The very reactive hydroxyl radical produced by deposition of ionizing radiation in water interacts with the bases or the sugar moieties of DNA. However, the step that leads directly to a DNA strand break is a hydrogen abstraction from deoxyribose. The sugar-centered radical produced in this process leads to a strand break by a β-cleavage of a phosphate bond neighboring the radical.

The process of H-abstraction by OH radical is a relatively simple atom transfer reaction in which the bond to the H atom is broken and a new bond to the OH is formed. According to Hammond's postulate,[14] the rates for H-abstraction should inversely correlate with the strength of the bond that is broken in the course of the reaction. The hydrogens in deoxyribose[15,16] can be classified into three categories on the basis of their bond strength. The α-hydrogens, which are attached to carbons with electronegative atoms on them, have the weakest bond strength; the β-hydrogens, which are one bond removed from the heteroatoms, have a stronger bond; the strongest bonds are of the oxy-hydrogens, which are bound to oxygens. In a previous study, the rates of hydrogen abstraction from methanol and ethanol by OH radical were calculated and found to agree with experimental data.[9] 2-Propanol is one of the simplest alcohols that contains the three types of hydrogens, and the α-hydrogen in it is attached to a tertiary carbon, like that in deoxyribose. Thus, 2-propanol can serve as a simplified model to study H-abstraction in deoxyribose.

In this study we have investigated all the possible reactions of hydrogen abstraction from 2-propanol by hydroxyl radical (•OH). These include three different processes determined primarily by the nature of the abstracted hydrogen and the products:

$$(CH_3)_2CHOH + {}^\bullet OH \rightarrow (CH_3)_2C^\bullet OH + H_2O \quad (H_\alpha\text{-abstraction}) \quad (1a)$$

$$(CH_3)_2CHOH + {}^\bullet OH \rightarrow CH_3CHOHC^\bullet H_2 + H_2O \quad (H_\beta\text{-abstraction}) \quad (1b)$$

$$(CH_3)_2CHOH + {}^\bullet OH \rightarrow (CH_3)_2CHO^\bullet + H_2O \quad (H_o\text{-abstraction}) \quad (1c)$$

An exhaustive search of all possible transition states for the three reactions yielded 16 pathways in total. The rate constants for each pathway, obtained from a treatment within the zero-curvature approximation of transition state theory including tunneling, yielded rate constants for each reaction channel as an average of all the relevant pathways. A comparison with experimental results can provide a critical evaluation of the theoretical approach described in the present work.

Early experimental measurements of the rate constant of H-abstraction in 2-propanol over a limited temperature range are available[17](see also a review by Atkinson[1,18]). More recently, the kinetics of H-abstraction from 2-propanol was measured over a wider temperature range.[19] Through the use of isotopic substitution the authors were able to determine the branching ratio between the abstraction of H_β and the combined abstraction of ($H_\alpha + H_o$) as a function of temperature. Their

† Present address: Department of Chemistry, Wesleyan University, Middletown, CT 06459.
* E-mail: osman@inka.mssm.edu.
⊗ Abstract published in *Advance ACS Abstracts,* January 1, 1997.

S1089-5639(96)02021-X CCC: $14.00

results clearly indicate a weak negative temperature dependence of the combined rate constant ($k_\alpha H + k_{OH}$) and a positive temperature dependence of the rate constant for the abstraction of H_β. Also, the rate constant of the abstraction of H_β shows a much larger kinetic isotope effect with a stronger temperature dependence than the combined rate constant for ($H_\alpha + H_o$) abstraction. The results presented in this work provide an opportunity to understand the molecular basis for the difference in the abstraction of the various hydrogens in complex molecules.

Methods

Structures and Energies. All *ab initio* quantum mechanical calculations were performed with GAUSSIAN 92.[20] The geometries of reactants, products and transition states were initially optimized with restricted or unrestricted Hartree−Fock methods, depending on the multiplicity of the electronic state of each species. The resulting geometries obtained with the 6-31G basis set were used for successive optimization at the HF/6-31G* and MP2/6-31G* levels. Inclusion of electron correlation significantly influenced structure optimization, and only structures optimized at the MP2/6-31G* level gave satisfactory results. Therefore, only results from calculations at this level are presented here. The optimized structure of each transition state has only one negative eigenvalue in its force constant matrix. Because the transition structures contain soft degrees of freedom, the tight convergence criterion in the GAUSSIAN program (i.e. convergence was accepted for maximum force 0.000 015 hartree/bohr or hartree/rad, and maximum displacement 0.000 060 bohr or rad) was applied to ensure better results in vibrational frequency analysis. Vibrational frequencies were calculated for each optimized structure at the same level of optimization. All orbitals for each species were included in the MP2 calculations.

The method of Gordon and Truhlar[4] was applied to scale the energies of all reactants, products, and transition states so that the bond dissociation energies of breaking 2-propanol into its radicals and H atom fit the experimental values.

Rate Constants. The rate constant for each pathway was calculated using the transition state theory with the quantum correction of the zero-curvature ground state approximation to tunneling (ZCG).[3,8]

The classical rate constant $k(T)$ in transition state theory is

$$k(T) = \frac{k_b T}{h} \frac{q_{TS}}{q_{OH}\, q_{ROH}} \exp\left[-\frac{V^f}{k_b T}\right] \qquad (2)$$

where k_b is the Boltzmann constant, T is temperature, h is the Planck constant, V^f is the forward potential energy barrier, and q's are the molecular partition functions for transition state complex (TS) or the reactant species (OH or ROH). Each of the molecular partition functions is assumed to be the product of electronic, translational, vibrational, and rotational partition functions of the corresponding species.

The rate constant that includes quantum tunneling at the zeroth-order approximation to the vibrational adiabatic potential energy surface model with zero-curvature can be calculated by approximating the potential energy curve with an unsymmetrical Eckart potential function:

$$V = -\frac{ay}{1-y} - \frac{by}{(1-y)^2} \qquad (3)$$

fitted through the zero-point-corrected energies of the reactants, transition states, and products, where

$$y = -e^{\lambda x} \qquad (4)$$

and λ is the range parameter and x the reaction coordinate.

The transmission probability $\kappa(E)$, obtained by solving the Schroedinger equation with the above Eckart potential function, is integrated to produce the rate constant that includes tunneling.

$$k_{tunn}(T) = \frac{1}{h} \frac{q_{TS}}{q_{OH}\, q_{ROH}} \int_0^\infty e^{-E/k_b T} \kappa(E)\, dE \qquad (5)$$

The tunneling correction is defined as the ratio between $k_{tunn}(T)$ and the classical rate constant $k(T)$.

The treatment of the complexity of the system of pathways, which lead from a mixture of reactants through a multiplicity of transition state structures to a distribution of products, can be simplified by the assumption that once a specific pathway has started, it will proceed to completion, independent of other pathways. In other words, there is no mixing or crossover between different pathways. This assumption allows us to decouple the reaction paths from each other and simplify the analysis. On the basis of this assumption, the total rate constant for the abstraction of a specific hydrogen is the average of the rate constants for the individual process weighted by the Boltzmann factors of the initial states. The total rate constant, which measures the rate of OH disappearance, is obtained by summing up the rate constants calculated for all pathways.[21]

Kinetic Isotope Effect. The kinetic isotope effect (KIE) with hydrogen substituted for deuterium is calculated as the ratio of the rate constant for the isotope-substituted species over that for the unsubstituted one. The former is calculated in the same way as described above, but with frequencies computed with isotope substitution on the same geometry as unsubstituted structures.

Results and Discussions

2-Propanol. Four distinct structures of 2-propanol with stationary energies were found by the optimization at the level of MP2/6-31G* (see the Supporting Information for the complete list of the geometric parameters of the optimized structures). They differ from each other in the orientation of the hydroxyl group with respect to the H_α. In two minimum energy conformers, the OH group is *gauche* and *anti* to H_α (see Scheme 1, C_α is in front of O), while in two maximum energy conformers, which form the barriers between the energy minima, the OH group is *syn* and *anticlinal* (*ac*) to H_α. The different orientations of the OH group result in small changes in the other structural parameters of the isomers as well. The bond lengths of the two minimum energy isomers are very similar to each other, and they agree well with previously optimized structures.[22]

The relative energies of all four conformers are listed in Table 1. The *anti* conformer is less stable by 0.15 kcal/mol than the *gauche* conformer at the MP2/6-31G* optimization level (corrected for ZPE), which is close to the experimental estimate of the energy difference in the range 0.02−0.49 kcal/mol in favor of the *gauche* conformer.[23,24] Previous studies calculated

SCHEME 1

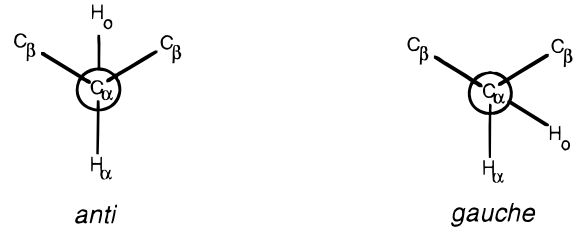

TABLE 1: Relative Energies of 2-Propanol Conformers and Isopropanolyl Radicals

2-Propanol Conformers with Stationary Energy

	anti	*ac*	*gauche*	*syn*
ΔE_{MP2}[a]	0.00	1.54	−0.16	1.48
ΔZPE[a]	0.00	−0.35	0.01	−0.40

2-Propanol Radicals

		β-radicals[b]				
	α-radical	*anti*, −*gauche*	+*gauche*, +*gauche*	−*gauche*, −*gauche*	−*gauche*, +*gauche*	oxy-radical
ΔE_{MP2}[c]	0	9.08	8.92	10.00	10.17	9.72
ΔZPE[c]	0	−0.83	−0.74	−1.08	−1.28	0.40

[a] The energies of 2-propanol conformers are relative to those of the *anti* conformer, which are $E_{MP2} = -193.706\,293$ hartrees; ZPE = 69.68 kcal/mol [b] The first label defines the torsion $H_oOC_\alpha H_\alpha$; the second label defines the torsional angle between the $C_\beta C_\alpha O$ plane and the direction of the unpaired electron calculated as half the sum of the torsional angles $H_\beta C_\beta$ $C_\alpha O$ of the remaining H_β on this carbon (see Scheme 2). [c] The energies of radical conformers are relative to the α-radical, whose energies are $E_{MP2} = -193.059\,868$ hartrees; E_{ZPE} = 61.019 kcal/mol.

the energy and structure of 2-propanol and its α-radical.[22,25−27] The results presented here are in good agreement with previous calculations, although none of the previous works attempted such high levels of optimization or energy calculations.

The energy difference between the *anti* and the *gauche* conformers is small. The rotational energy barriers that separate these nearly degenerate states are also not high. The energy barriers at the dihedral angle of the hydroxyl group relative to H_α equal to 0 (*syn*) and 120 (*ac*) are 1.19 and 1.08 kcal/mol (corrected for ZPE), respectively, relative to the energy of the *anti* isomer.

Isopropyl Radicals. Six distinctive 2-propanol radicals were identified as stable products of the H-abstraction reaction. One each for α- and oxy-radicals and four for *β*-radical. The only conformer of the α-radical found is that where the hydroxyl group is *gauche* to the unpaired electron; the *anti* conformer is not stable, possibly because the unpaired electron staggered between the oxygen lone pairs increases too much the electron−electron repulsion. By symmetry, only one oxy-radical is possible. Four stable *β*-radical conformers have been found after systematic search of the $H_oOC_\alpha H_\alpha$ dihedral angle conformation with the position of the *β*-hydrogen being abstracted. These could be classified as (*anti*, −*gauche*), (+*gauche*, +*gauche*), (−*gauche*, −*gauche*), and (−*gauche*, +*gauche*). The first label refers to the $H_oOC_\alpha H_\alpha$ dihedral angle, demonstrated in the first row of Scheme 2 (C_α is in front of O). The second label indicates the orientation of the unpaired electron on C_β relative to O, calculated as half the sum of the torsional angles of the remaining H_β on this carbon. This is illustrated in the second row of Scheme 2 (C_β is in front of C_α).

The energies of the isopropyl radicals are shown relative to the α-radical in Table 1. The *β*-radicals are 8−9 kcal/mol less stable and the oxy-radical is about 10 kcal/mol less stable than the α-radical. The four separate *β*-radicals can be divided into two groups of two each, with the first group more stable by approximately 0.7 kcal/mol than the other. Apparently, the proximity of the oxy-hydrogen to the unpaired electron on the *β*-carbon differentiates the two groups. In both (*anti*, −*gauche*) and (+*gauche*, +*gauche*), which are the more stable, the H_o is closer to the unpaired electron, whereas in the other two isomers the unpaired electron is nearly staggered between the lone pairs on the oxygen.

Bond Dissociation Energy and Scaling of Correlation Energy. The bond dissociation energies for H_α-, H_β-, and H_o-abstractions, calculated from the energies in Tables 1 are 93.1, 102.7, and 102.8 kcal/mol, respectively. The experimental enthalpies at 298.15 K are 91.1, 102.4, and 104.8 kcal/mol, respectively.[19,28−30] To compare them with the calculated values, we convert the experimental quantities to values at 0 K and then subtract the zero-point vibrational energies.[31] The resultant values are 98.4, 110.9, and 112.3 kcal/mol, clearly showing that the MP2 values are underestimating the bond energies because they recover only a portion of electron correlation energy. It has been shown[4,10,32] that the full correlation energy can be approximated by a linear scaling:

$$E_{corr} = E_{HF} + (E_{MP2} - E_{HF})/F \qquad (6)$$

The scaling factor F is dependent on the nature of the particular bond that changes in the chemical process, but is assumed to be independent of the overall geometry of the molecules involved. Thus, the scaling factor can be used to adjust the energies of the transition state structures.

The scaling factors for H_α, H_β, and H_o bond breaking are 0.75, 0.68, and 0.76, respectively. In the following calculation of transition state energy barriers, all the MP2 energy values are scaled with the above scaling factors and are denoted as the MP-SAC2 energies.

Transition States. An exhaustive search produced a total of 16 transition state structures shown in Figures 1−5, together with some key geometric parameters. The energies relative to the corresponding reactant state, as well as the imaginary frequency and the dipole moment for each of these structures, are shown in Table 2. Complete information on geometries of these structures can be found in the Supporting Information.

To compare the effects of computational methods (HF vs MP2) and the effects of basis sets (6-31G vs 6-31G*) in obtaining the optimized structure, all reactants, products, and transition state structures involved in the H_α-abstraction have been optimized at four different levels. The forward energy barrier for H_α-abstraction is negative at the level of MP2/6-31G* calculation if the structures are optimized at the HF/6-31G* level. This can be avoided when electron correlation is included (MP2) during optimization, indicating that election correlation is important in obtaining qualitatively correct energy barriers. Therefore, all subsequent discussions focus on results of MP2/6-31G* level calculations.

(1) H_α-Abstraction. There are three possible transition state structures for the abstraction of the α-hydrogen in 2-propanol distinguished by the dihedral angle of $H_oOC_\alpha H_\alpha$: −*gauche*, +*gauche*, and *anti*. However, the two *gauche* structures are symmetric, reducing the number of unique transition state structures for this process to two. The transition state structures are shown in Figure 1, with the structural and energetic information as well as imaginary frequencies and dipole moments in Table 2.

Two major changes occur upon the approach of OH radical to form a transition state for H_α-abstraction. One is the elongation of the $C_\alpha H_\alpha$ bond, and the other is the associated shortening of the surrounding bonds, e.g. $C_\alpha O$ and $C_\alpha C_\beta$. The shortening is small and approximately 0.01−0.02 Å, but the elongation of the $C_\alpha H_\alpha$ bond is a sensitive measure for the formation of the transition state along the reaction coordinate. For example, $C_\alpha H_\alpha$ in *gauche* is elongated by 0.086 Å, whereas in *anti* it is elongated by 0.105 Å. This suggest an earlier transition state for the *gauche* isomer and is in clear agreement with the longer distance of approach of the OH radical, which is 2.507 Å as compared to 2.474 Å in the *anti* isomer (see Figure

SCHEME 2

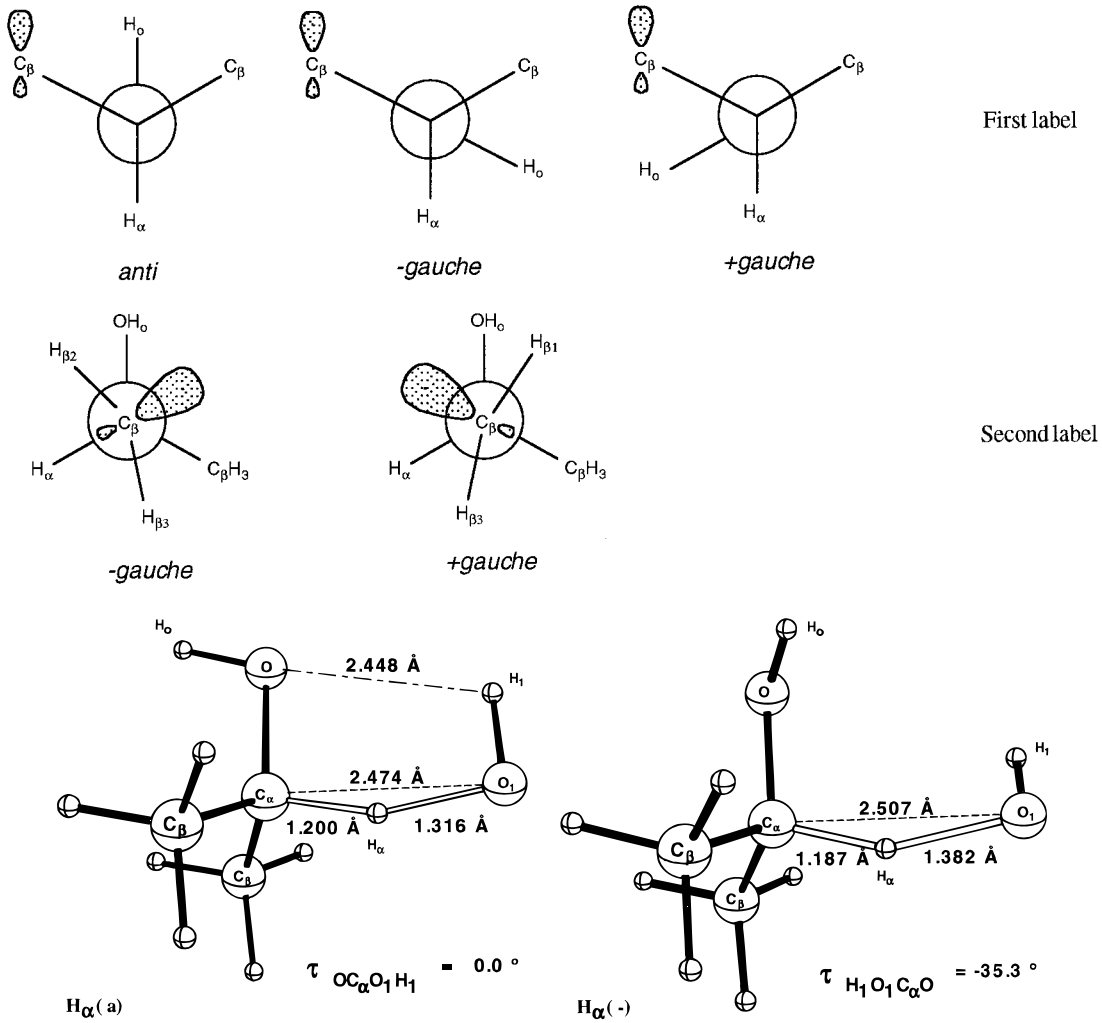

Figure 1. Structures of the two transition states for H_α-abstraction: H_α(a), *anti*; H_α(−), *−gauche*.

1). The later occurrence of the transition state is also consistent with Hammond's postulate that the barrier for H-abstraction in the *anti* isomer is 1.23 kcal/mol higher than that of the *gauche* isomer (Table 2). Some of the local properties of the barrier around a transition state along the reaction coordinate are reflected in the imaginary frequency shown in Table 2. The imaginary frequency of the *gauche* transition state is smaller by nearly 350 cm^{-1} than the *anti*, indicating that the barrier is wider and thus reducing the effect of tunneling on the rate constant (see below).

(2) H_β-Abstraction. The number of possible transition state structures in the abstraction of H_β increases drastically compared to that of H_α-abstraction. One reason for the increased complexity is the elimination of the intrinsic symmetry of H_α, which is positioned in the plane that reflects one half of the molecule into the other. Thus, while the two *gauche* conformations in the transition states of H_α-abstraction are degenerate with respect to this plane, the transition states for H_β-abstraction no longer have this property, leading to three possible transition states due to the isomers of the hydroxyl group. Another reason for the increased complexity is that in each of the transition states due to isomerism of the hydroxyl group the orientation of H_β can take three possible positions. Finally, the possibility of forming two different types of hydrogen bonds between the hydroxyl group and the OH radical contributes an additional level of complexity.

We have identified 11 distinct H_β-abstraction transition states, which can be classified into three groups. The structures are shown in Figures 2, 3, and 4, and their properties are listed in Table 2. The first group (Figure 2) includes four transition state structures in which the hydrogen of the OH radical, H_1, is H-bonded to the oxygen of the hydroxyl group of 2-propanol, O. The second group (Figure 3) includes three structures in which the hydrogen of the hydroxyl group of 2-propanol, H_o, makes an H-bond with the oxygen of the OH radical, O_1. The third group (Figure 4) includes four structures in which the OH radical abstracts an H_β that is *anti* to the hydroxyl group of the 2-propanol; thus no hydrogen bond can be formed. Because the scaling factors for the correlation energy calculated above were obtained from bond dissociation energies, the hydrogen bond energy contribution was excluded from the energy scaling for the first two groups of H_β-abstraction. We noted that the MP2 barriers with the hydrogen bond are lower by about 3.4 kcal/mol. This amount of energy is taken out before scaling and added back to the energy. Namely, eq 6 for scaling is modified as

$$E_{corr} \approx (E_{HF} + \Delta E_{H-bond}) + \frac{E_{MP2} - (E_{HF} + \Delta E_{H-bond})}{F} \quad (7)$$

The resultant barriers are similar for all pathways and are higher than those for H_α-abstraction.

Similar to the H_α-abstraction, the major structural changes in the course of H_β-abstraction relative to 2-propanol are

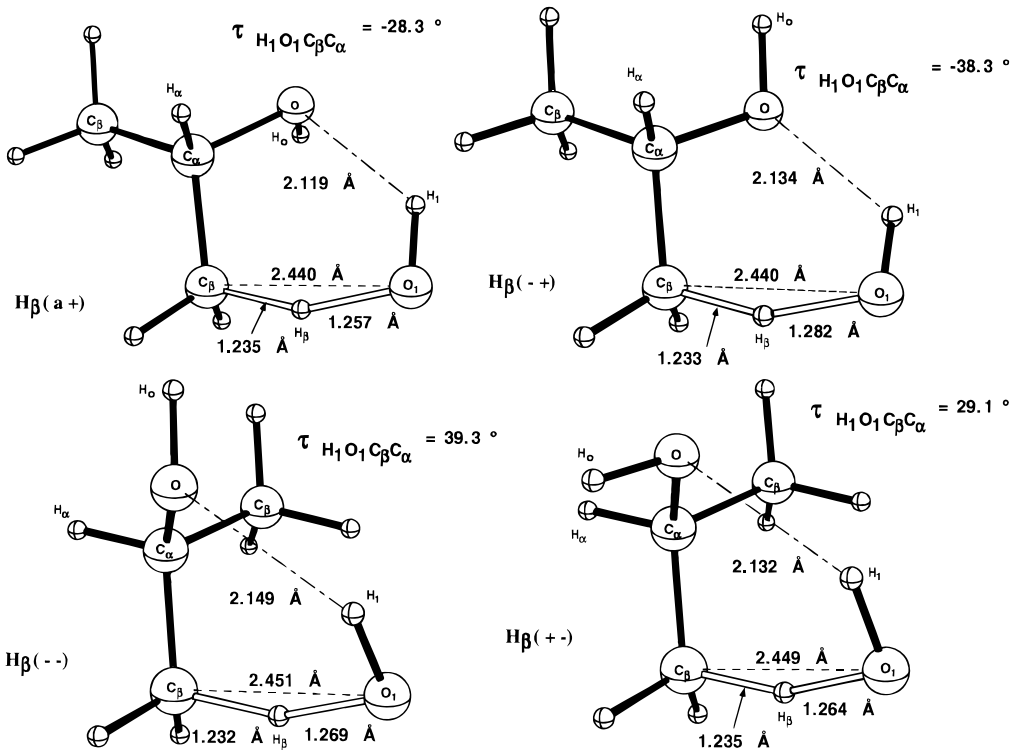

Figure 2. Structures of the four transition states for H_β-abstraction with hydrogen bonding between H_1 and O: H_β(a+), (*anti*, +*gauche*); H_β(− +), (−*gauche*, +*gauche*); H_β(− −), (−*gauche*, −*gauche*); H_β(+ −), (+*gauche*, −*gauche*).

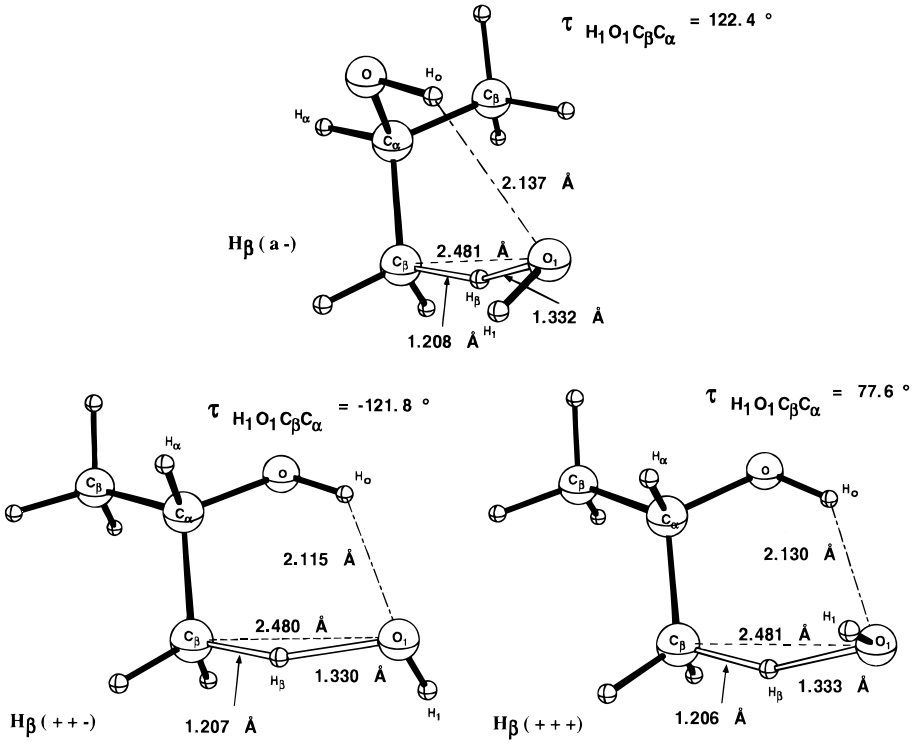

Figure 3. Structures of the three transition states for H_β-abstraction with hydrogen bonding between H_o and O_1: H_β(a−), (*anti*, −*gauche*); H_β(+ + −), (+*gauche*, +*gauche*, −*gauche*); H_β(+ + +), (+*gauche*, +*gauche*, +*gauche*).

localized around the bond between the abstracted hydrogen, $H_{\beta a}$, and the carbon next to it, C_β. The increase in the $C_\beta H_{\beta a}$ bond length and the distance of approach of O_1 to C_β report about the position of the transition state along the reaction coordinate. Within each group there are subtle structural differences, which appear to originate from other factors than the position of the transition state along the reaction coordinate. We therefore averaged the $C_\beta H_{\beta a}$ and the O_1C_β distances and related them to the averaged barrier height. In the first group (Figure 2), the increase in $C_\beta H_{\beta a}$ is on the average 0.141 ± 0.002 Å and the average distance of approach of the OH radical to C_β is 2.445 ± 0.006 Å. The average scaled energy barrier for this group is 2.81 ± 0.45 kcal/mol (Table 2). In the second group (Figure 3), the average increase in $C_\beta H_{\beta a}$ is 0.114 ± 0.002 Å and the average distance of approach is 2.481 ± 0.001 Å. The corresponding average energy barrier for this group is 3.13 ± 0.39 kcal/mol (Table 2). In the third group (Figure 4), the average increase in $C_\beta H_{\beta a}$ is 0.121 Å, which lies between the

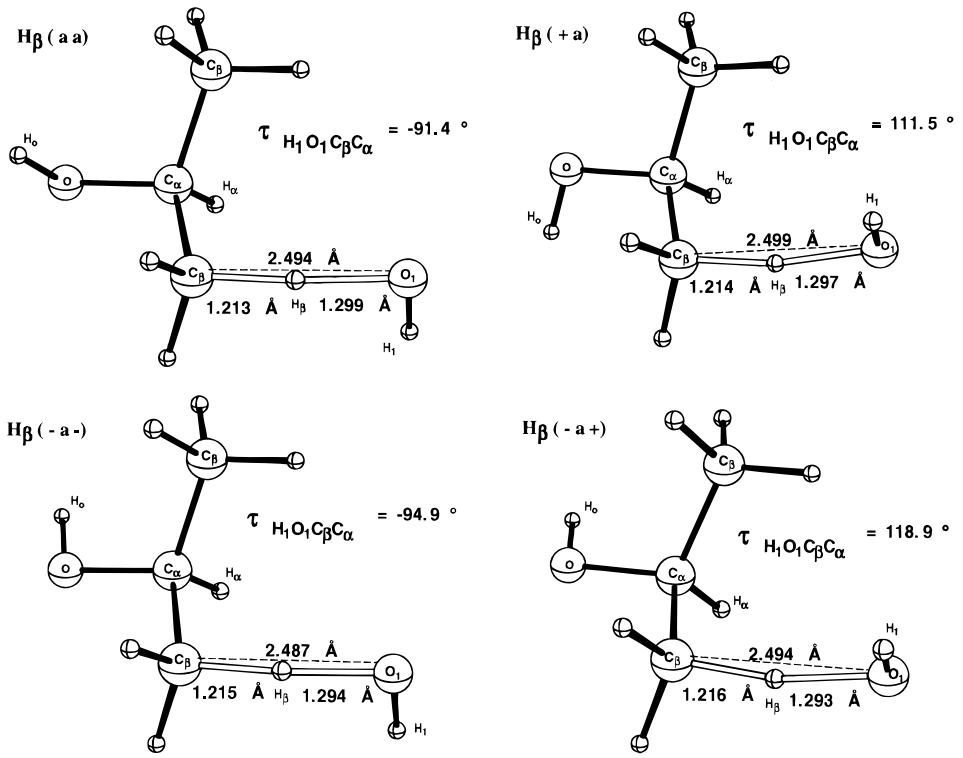

Figure 4. Structures of the four transition states for H_β-abstraction without hydrogen bonding: H_β(aa), (*anti*, *anti*); H_β(+a), (+*gauche*, *anti*); H_β(−a−), (−*gauche*, *anti*, −*gauche*); H_β(−a+), (−*gauche*, *anti*, +*gauche*).

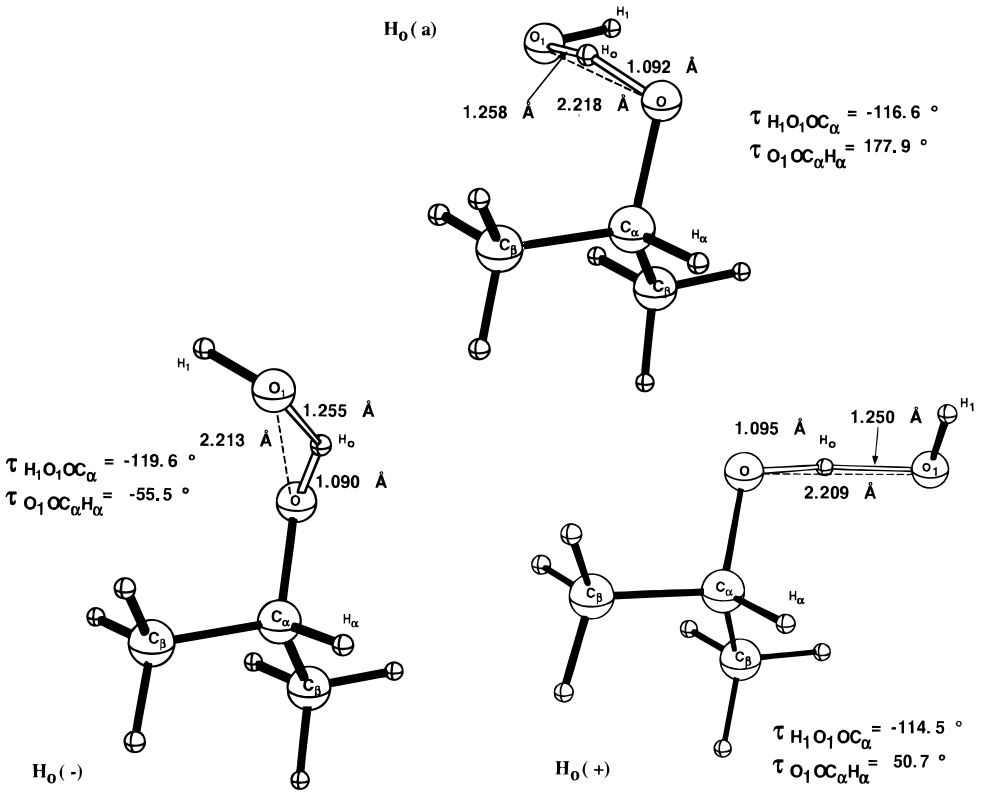

Figure 5. Structures of the three transition states for H_o-abstraction: H_o(a), *anti*; H_o(−), −*gauche*; H_o(+), +*gauche*.

increases observed in the two previous groups. On the other hand, the average approach distance is 2.494 ± 0.006 Å, which is the longest among the three groups. Judging only on the basis of the O_1C_β approach, the transition state in the third group occurs at the earliest point along the reaction coordinate. The average barrier, however, is 3.68 ± 0.07 kcal/mol (Table 2). It appears that the third group has a higher barrier because of the absence of the intramolecular hydrogen bond present in the other two groups. However, Hammond's postulate does not hold in these cases, possibly because the reaction coordinates are not comparable.

The analysis of the ZPE difference between the transition states and reactants shows that the first two groups have average ZPEs around −0.9 kcal/mol, whereas the average ZPE in the third group is twice as much (−1.8 kcal/mol). This originates from the restriction of two torsional degrees of freedom,

TABLE 2: Energy Barriers, Imaginary Frequencies and Dipole Moments of Transition States

	structure[a]	$\Delta E_{MP-SAC2}$[b]	ΔZPE[b]	ν_{im} (cm^{-1})	μ (D)
H_α-abstraction					
	anti	1.35	−1.91	1936.83	2.3638
	gauche	0.12	−1.26	1583.05	0.5490
H_β-abstraction					
$O-H_1$ H-bond					
	anti, +*gauche*	3.15	−1.03	2312.77i	2.9368
	−*gauche*, +*gauche*	3.25	−1.07	2282.51i	3.2951
	−*gauche*, −*gauche*	2.37	−0.95	2269.37i	3.1413
	+*gauche*, −*gauche*	2.47	−0.90	2301.80i	2.7033
O_1-H_o H-bond					
	anti, −*gauche*	2.80	−0.78	1955.90i	2.1520
	+*gauche*, +*gauche*, −*gauche*	3.03	−0.80	1969.90i	2.1622
	+*gauche*, +*gauche*, +*gauche*	3.56	−0.88	1949.51*i*	3.0220
no H-bond					
	anti, *anti*	3.62	−1.77	2085.59i	0.8587
	+*gauche*, *anti*	3.65	−1.77	2107.42i	1.3916
	−*gauche*, *anti*, −*gauche*	3.77	−1.84	2068.68i	1.9123
	−*gauche*, *anti*, +*gauche*	3.66	−1.82	2083.09i	1.6062
H_o-abstraction					
	anti	1.93	−0.70	2853.02i	1.4457
	−*gauche*	1.68	−0.75	2859.04i	1.4016
	+*gauche*	1.92	−0.78	2778.24i	1.4550

[a] In all structures, the first label defines the torsion $H_oOC_\alpha H_\alpha$; in H_β-abstraction, the second label defines the torsion $H_{\beta a}C_\beta C_\alpha O$, where $H_{\beta a}$ is the β-hydrogen being abstracted, and the third label defines the torsion $H_1O_1H_{\beta a}C_\beta$. [b] All energies are relative to those of corresponding reactants.

TABLE 3: Rate Constants and Quantum Tunneling at 300 K

transition state	channel R, P[a]	classical rate constant[b] (10^{-13} cm^3 molecule^{-1} s^{-1})	tunneling correction	ZCG rate constant[c] (10^{-13} cm^3 molecule^{-1} s^{-1})
Hα (a)	(a), (−)	$1.68 \times 10^{+1}$		16.8
Hα (−)	(−), (−)	$3.26 \times 10^{+1}$		32.6
Hβ (a+)	(a), (a−)	4.50×10^{-2}	5.63	0.254
Hβ (− +)	(−), (− +)	4.05×10^{-2}	5.85	0.237
Hβ (− −)	(−), (− −)	9.63×10^{-2}	3.22	0.310
Hβ (+ −)	(+), (+ +)	7.42×10^{-2}	3.69	0.274
Hβ (a−)	(a), (a−)	4.89×10^{-2}	4.40	0.215
Hβ (+ + −)	(+), (+ +)	3.84×10^{-2}	5.04	0.193
Hβ (+ + +)	(+), (+ +)	1.76×10^{-2}	6.28	0.111
Hβ (aa)	(a), (a−)	2.56×10^{-1}	3.70	0.949
Hβ (+a)	(+), (+ +)	2.07×10^{-1}	3.79	0.784
Hβ (−a−)	(−), (− −)	2.30×10^{-1}	3.86	0.886
Hβ (−a+)	(−), (− −)	2.22×10^{-1}	3.68	0.816
H*o* (a)	(a), (o)	3.22×10^{-1}	2.48	0.799
H*o* (−)	(−), (o)	3.21×10^{-1}	3.12	1.00
H*o* (+)	(+), (o)	3.49×10^{-1}	3.00	1.05

[a] R and P are the reactant and product channel corresponding to the transition state. [b] Classical rate constant calculated with eq 2. [c] Rate constant $k(T)$ at $T = 300$ K is calculated using the ZPE-corrected MP-SAC2 barrier with quantum tunneling.

$H_oOC_\alpha H_\alpha$ and $H_\beta C_\beta C_\alpha O$, which in 2-propanol had low frequencies that contributed significantly to lowering of the ZPE but are not present in the transition state. In the third group, where such a restriction is not present, these degrees of freedom are similar in the reactants and the transition state and thus do not increase the ZPE difference.

(3) H_o-Abstraction. The three distinct transition state structures of H_o-abstraction are shown in Figure 5, and their structural parameters, energetic information, and imaginary frequencies and dipole moments are listed in Table 2. The structures are very similar to each other, differing primarily in the orientation of the OH group, which also defines the position of the •OH radical. The barriers of the three transition state pathways are also very similar to each other.

In summary, the classical barriers are divided into three groups at the MP-SAC2 level. H_α-abstraction has the lowest barriers around 1 kcal/mol. H_o-abstraction's barriers are nearly 2 kcal/mol. H_β-abstraction has average barriers around 3 kcal/mol.

Rate Constants. The rate constants as a function of temperature are calculated at the ZCG level of approximation, which includes quantum tunneling (eq 5). The values of the rate constants for each pathway at 300 K are listed in Table 3. For comparison, the classical rate constant (eq 2) and the quantum tunneling correction at the same temperature are also provided. The values in Table 3 are based on the ZPE-corrected barriers calculated at the MP-SAC2/6-31G* level with frequencies at the MP2/6-31G* level. The 16 pathways can be divided into four distinct categories based on their structural characteristics. The H_α-abstraction, with the lowest energy barriers, gives the highest classical rate constant. The next group consists of the H_β-abstractions with hydrogen bonding in the transition state; in this group the classical rate constants are about 3 orders of magnitude smaller than those in the first category. The third category, H_β-abstraction without hydrogen bonding in the transition state, and the fourth category of H_o-abstraction have essentially the same rate constants, which are about 1 order of magnitude larger than the second group.

The dominant factor that determines the classical rate constant is the barrier height including the ZPE correction, as illustrated above in the division of the rate constants for the 16 pathways into three groups, each with a characteristic order of magnitude

determined by barrier height. The *gauche* pathway in H_α-abstraction has a very low barrier of 0.12 kcal/mol, which is within the thermal energy range. It is conceivable that the reaction proceeding along this pathway is nearly collision controlled. In fact, the extremely weak temperature dependence of the experimental kinetic isotope effect for H_α-abstraction (see below) is also consistent with the collisional mechanism. The collision-controlled reaction rate constant can be calculated by multiplying the collision rate constant k_{col} of two spherical reactants with the fractions of accessible surfaces of the reactive centers in each reactant f_i:

$$k = f_{2-\text{propanol}} f_{OH} k_{col} \tag{8}$$

with[33]

$$k_{col} = (\pi d_{AB}{}^2)(8k_b T/\pi\mu)^{1/2} \tag{9}$$

where d_{AB} is the collision diameter, $\mu = 13.25$ au is the reduced mass, k_b is the Boltzmann constant, and T is temperature. Here we have assumed that the collision-controlled reaction rate constant is proportional to the fraction of accessible surface of each reactive center (such as H_α in H_α-abstraction) within the accessible surface of the entire molecule (2-propanol). For H_α-abstraction by OH radical, $f_{2-\text{propanol}} = 0.11$, and $f_{OH} = 0.55$. If we take $d_{AB} \approx 4.0$ Å on the basis of molecular diameters derived from measurement of gas viscosity,[34] the collision-controlled rate constant at 300 K is 2.1×10^{-11} cm^3 s^{-1} molecule^{-1}, which is about 5 times the experimental value. On the other hand, if we use $d_{AB} \approx 2.5$ Å, the separation of C_α and OH in the transition state, then the collision-controlled rate constant will be 8.2×10^{-12} cm^3 s^{-1} molecule^{-1}, only twice the experimental value.

Two pathways with a similar potential energy barrier can have different classical rate constants because of the product of their partition functions. The major differences between partition functions of different pathways originate from the transition state soft vibrational modes with frequencies below the thermal motion frequency, which at 300 K is about 210 cm^{-1}. Therefore, the number and values of the frequencies below that threshold will be a major factor in determining the partition function at 300 K. For example, each pathway of the H_β-abstraction without hydrogen bonding in the transition state has three soft modes, while that of the H_β-abstractions with hydrogen bonding in the transition state has only two. Thus, although these two categories have about the same range of barrier heights, the partition functions of the former are about 3−5 times larger than the latter. This brings the classical rate constants for the H_β-abstraction without hydrogen bonding in the transition state into the same range as those of the H_o-abstraction, which has a barrier about 0.7 kcal/mol lower, but has only two soft vibrational modes for each transition state structure.

Although the classical rate constants are spread over 3 orders of magnitude, the inclusion of tunneling brings the rate constants for all pathways to within 2 orders of magnitude. This illustrates the significance of the tunneling contribution, which depends on, among others, the imaginary frequency ν_{im} at the transition state. For example, the H_β (− +) pathway, with the same barrier as H_β (+ + −), of about 2.2 kcal/mol after ZPE correction (see Table 2), has a larger tunneling correction of 5.85 compared to 5.04 for H_β (+ + −) (see Table 3). This is because the H_β (− +) pathway has a higher imaginary frequency, or narrower barrier, than H_β (+ + −). The tunneling correction also depends on barrier height in a complicated manner. Therefore, two pathways having similar imaginary frequencies may have quite different tunneling corrections if their barrier heights differ significantly. For example, the imaginary frequencies of H_β (− +) and H_β (− −) are 2283 and 2269 cm^{-1}, respectively (Table 2), but their tunneling corrections are 5.85 and 3.22 (Table 3). This is because their barrier heights are 2.2 and 1.4 kcal/mol after ZPE correction (Table 2).

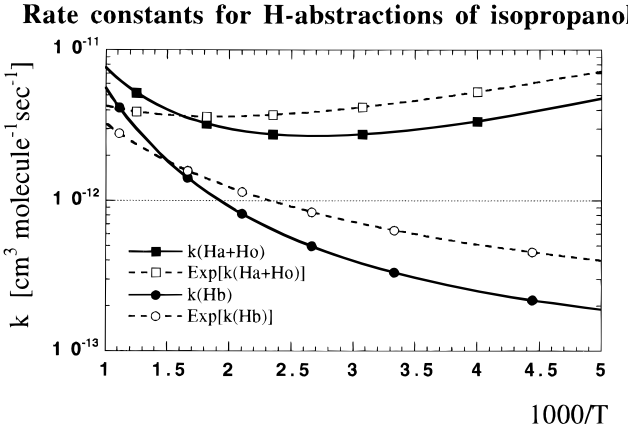

Figure 6. Calculated rate constant for ($H_\alpha + H_o$) and H_β-abstractions with quantum tunneling and ZPE correction comparing with the experimental rate constants.

The average rate constant for each hydrogen abstraction reaction channel (e.g., the H_α-abstraction) is the sum of the rate constants for all pathways in that channel weighted by the Boltzmann factor of their corresponding reactants. The *gauche* pathway contributes about four-fifths in the H_α-abstraction rate constant. The four H_β-abstraction pathways without hydrogen bonding in the transition state contribute about 70% to the H_β-abstraction rate constant. In Figure 6, the rate constants for the combined ($H_\alpha + H_o$) abstraction channel and the H_β-abstraction channel are plotted as a function of temperature and are compared with recommended experimental values of Dunlop and Tully.[19] The calculated rate constants are in close agreement with the experiment results. The predictions for both ($H_\alpha + H_o$) abstraction and H_β-abstraction at 300 K differ from experiment by a factor less than 2. In addition, the calculated ($H_\alpha + H_o$) abstraction rate constant exhibits the same reverse temperature dependence as observed experimentally in the low-temperature range of $T < 350$ K. This indicates that the dominant reaction has a very low barrier and is entering the collision-controlled regime. H_β-abstraction shows a more regular temperature dependence. Both calculated rate constants are a little lower than those of the experimental values. There are several approximations introduced in the calculation that may account for the discrepancy. The zero-curvature approximation applied in this work may underestimate the rate constant. The assumption that all the pathways proceed independently also leads to underestimation because the contributions from crossing different pathways are neglected. In view of the close agreement with the experimental results, these assumptions, which greatly reduce the computations, appear to be justified.

Kinetic Isotope Effect. The KIE for the combined channel of ($H_\alpha + H_o$) abstraction and for H_β-abstraction are displayed in Figure 7a,b. The KIE for H_β-abstraction is in very good agreement with experiment in both the numerical value and the temperature dependence. The theoretically calculated KIE for ($H_\alpha + H_o$) abstraction has a higher slope than the experimental one. This may indicate that the potential energy surface near the very low barrier is highly anharmonic and would require a more rigorous evaluation of the vibrational properties. Alternatively, this may suggest that transition state theory is breaking down as the reaction proceeds in this very low barrier region, where the reaction is nearly collision controlled.

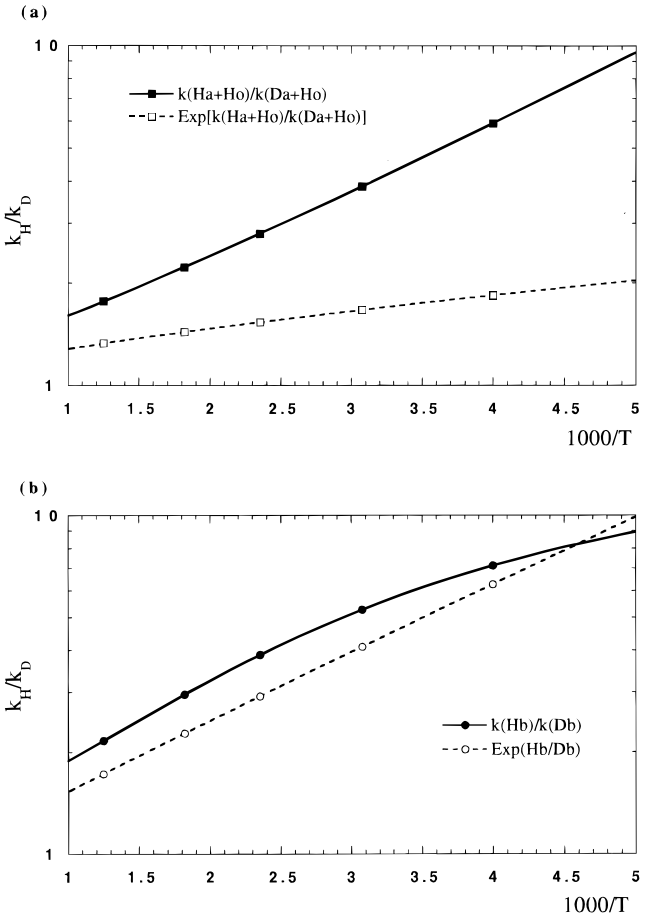

Figure 7. (a) Kinetic isotope effect of (H_α + H_o) abstraction. (b) Kinetic isotope effect of H_β-abstraction.

Implications for Large Systems and Systems in Solution. Our long-range goal is to investigate H-abstraction from deoxyribose. From the present study, it is clear that the number of transition states will increase rapidly as the system increases in size. Consequently, the determination of every transition state, which depends on the intricate details of the molecular structure and the local properties of the potential energy surface, will become prohibitive. It is therefore pertinent to be able to estimate the rate constant from as few quantum calculations of transition states as possible. Our results show that within each category of H-abstraction the contributions of the various pathways to the rate constant are very close to each other. Therefore, if we restrict ourselves to calculate one transition state structure and energy for each category, the rate constant for a specific category can be estimated by the product of the multiplicity of the pathways in the specific category and the rate constant of one pathway in that category. The multiplicity for each of the categories in the H-abstraction of 2-propanol can be easily determined if we ignore the different possible orientations in the attacking •OH group. For example, the multiplicities for H_α-abstraction and H_o-abstraction are both 3, corresponding to the three orientations of the OH_o of the 2-propanol (*anti*, +*gauche*, and −*gauche*). The situation with the H_β-abstraction is more involved because of the lower symmetry of the transition state structures. We can analyze the abstraction from one of the C_β and subsequently multiply the resulting number of channels by 2 because of the presence of the equivalent processes on the other C_β. Similarly to the H_α- and H_o-abstraction, the multiplicity of the abstraction of H_β without an intramolecular hydrogen bonding in the transition state is 3. The fourth transition state structure identified in our work represents a different orientation of the OH radical. The possible situation for H_β-abstraction with an intramolecular hydrogen bonding are shown in Scheme 3. There are four ways to form a hydrogen bond between H_1 of the OH radical and O of 2-propanol in the transition structure; these are shown in the top two lines of Scheme 3. Whether the abstraction is of $H_{\beta1}$ (−*gauche* to O) or $H_{\beta2}$ (+*gauche* to O), H_1 can form a hydrogen bond with O only in two different orientations of the OH_o: −*gauche* and +*gauche* for $H_{\beta1}$-abstraction and *anti* and −*gauche* for $H_{\beta2}$-abstraction. There are only two ways to form a hydrogen bond between H_o of 2-propanol and the OH radical. One possibility is in $H_{\beta1}$-abstraction (−*gauche* to O), which positions H_o in an *anti* orientation. The other is in $H_{\beta2}$-abstraction (+*gauche* to O), which positions H_o in a +*gauche* orientation. Thus, there are 12 possibilities of abstracting H_β with an intramolecular hydrogen bond and six possibilities without a hydrogen bond.

The rate constant of H_β-abstraction, for example, can now be estimated in the following way. The difference between the two states of the reactants (*gauche* and *anti* conformers of 2-propanol) is sufficiently small and can be neglected to yield an equal population. To obtain an upper bound estimate of the rate constant, we select the highest rate constant from the category, which is of the pathway H_β (aa), and multiply it by the multiplicity of pathways, which is 11. In a similar way we obtain the lower bound estimate by selecting the lowest rate constant in the category, which is of the pathway H_β (+ + +), multiplying it by 11. The range of this estimation is (1.22−10.44) × 10^{-13} cm^3 $molecule^{-1}$ s^{-1} at 300 K. This illustrates that the rate constant can be estimated within an order of magnitude with such an approximate method.

The reaction dynamics of H-abstraction in aqueous solution could be influenced by several other factors. One important aspect is the stabilization of the transition state by the highly polar aqueous environment, which should be directly proportional to the dipole moment in the transition state. For example, the dipole moment of the *anti* form of H_α-abstraction is 2.36 D compared to 0.55 D for the *gauche* form. This should enhance the abstraction in the *anti* form compared to that in the *gauche* form and bring the two rate constants closer to each other. In such a situation the selection of only one representative transition state structure for H_α-abstraction is very adequate. Another likely change, which would contribute significantly to the simplification of the H_β-abstraction channels, comes from the possible destabilization of the hydrogen-bonded transition state structures compared to those without the hydrogen bond. In this case the analysis of the various possibilities may lead to a coalescence of different pathways, lending greater relevance to the analysis presented above. We are now in the process of evaluating the effect of solvation on the potential energy surfaces of H-abstraction.

Conclusions

We have presented in this paper a detailed analysis of hydrogen abstraction from 2-propanol by •OH radical. The level of quantum mechanical calculation used in geometry optimization has significant effects on the energy profiles. Inclusion of electron correlation during structure optimization can produce a qualitative change in the characteristics of the energy barriers and a substantial quantitative change in the imaginary frequencies.

As our study demonstrates, the number of transition state structures increases rapidly with the increase in the size of the molecular system. However, they can be grouped according to the type of hydrogen abstracted and whether or not a hydrogen

SCHEME 3

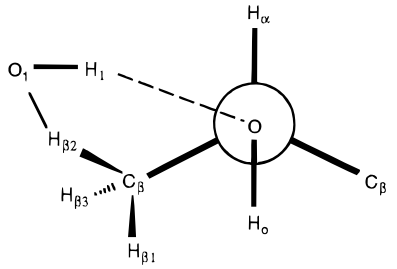

(anti, +gauche)

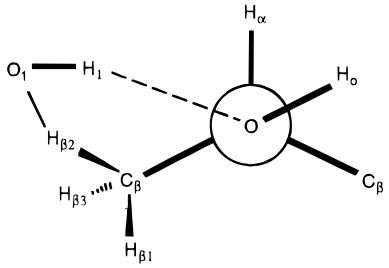

(-gauche, +gauche)

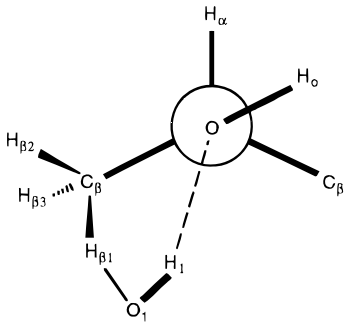

(-gauche, -gauche)

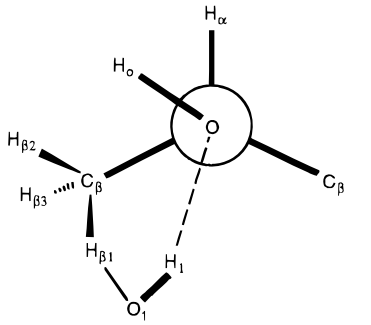

(+gauche, -gauche)

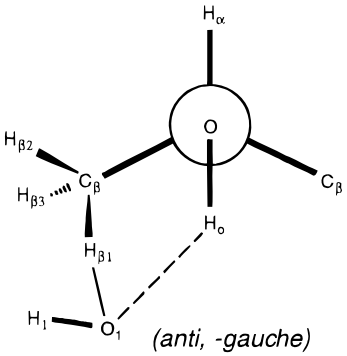

(anti, -gauche)

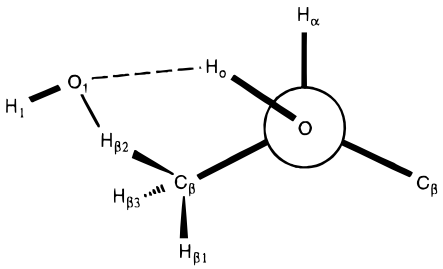

(+gauche, +gauche)

bond is formed in the transition state. Within each group, the differences in the energies of the transition states and the rate constant corresponding to each pathway are small. Such a simplification of the number of transition state structures that need to be calculated presents a manageable approach to the calculation of the rate constants for H-abstraction in complex molecules.

The calculated rate constant and KIE for the H_β-abstraction at the level of computation presented in this work agree with the experimental data very well. Our analysis suggests that the collision-controlled mechanism may play a significant role in the H_α-abstraction.

The gas-phase study presented in this work forms a starting point for our future studies of hydrogen abstraction from DNA in aqueous solution.

Acknowledgment. This research was supported in part by US PHS Grant CA 63317. We thank the National Energy Research Supercomputer Center at Lawrence Livermore National Laboratory for providing computational support for this work.

Supporting Information Available: Detailed description of the geometric parameters of all structures obtained in this work by computation, including bond lengths, bond angles, and dihedral angles (8 pages). Ordering information is given on any current masthead page.

References and Notes

(1) Atkinson, R. *J. Phys. Chem. Ref. Data* **1989**, Monograph 1, 160−1.
(2) Walch, S. P.; Dunning, T. H., Jr. *J. Chem. Phys.* **1980**, *72*, 1303−11.
(3) Truong, T. N.; Truhlar, D. G. *J. Chem. Phys.* **1990**, *93*, 1761−69.
(4) Gordon, M. S.; Truhlar, D. G. *J. Am. Chem. Soc.* **1986**, *108*, 5412−19.
(5) Dunning, T. H., Jr.; Harding, L. B.; Bair, R. A.; Eades, R. A.; Shepard, R. L. *J. Phys. Chem.* **1986**, *90*, 344−56.
(6) Dupuis, M.; Lester, W. A., Jr. *J. Chem. Phys.* **1984**, *81*, 847−50.
(7) Gonzalez, C.; McDouall, J. J. W.; Schlegel, H. B. *J. Phys. Chem.* **1990**, *94*, 7467−71.
(8) Gonzalez-Lafont, A.; Truong, T. N.; Truhlar, D. G. *J. Chem. Phys* **1991**, *95*, 8875−94.
(9) Pardo, L.; Banfelder, J.; Osman, R. *J. Am. Chem. Soc.* **1992**, *114*, 2382−90.
(10) Melissas, V. S.; Truhlar, D. G. *J. Chem. Phys.* **1993**, *99*, 1013−27.
(11) Melissas, V. S.; Truhlar, D. G. *J. Phys. Chem.* **1994**, *98*, 875−86.
(12) Melissas, V. S.; Truhlar, D. G. *J. Chem. Phys.* **1993**, *99*, 3542−52.
(13) von Sonntag, C. *The Chemical Basis of Radiation Biology*; Taylor & Francis: London, 1987.
(14) Hammond, G. S. *J. Am. Chem. Soc* **1955**, *77*, 334.
(15) Miaskiewicz, K.; Osman, R. *J. Am. Chem. Soc.* **1994**, *116*, 232−8.

(16) Colson, A.-O.; Sevilla, M. D. *J. Phys. Chem.* **1995**, *99*, 3867−74.
(17) Wallington, T. J.; Kurylo, M. J. **1987**, *19*, 1015.
(18) Atkinson, R. *Chem. Rev.* **1985**, *85*, 69−201.
(19) Dunlop, J. R.; Tully, F. P. *J. Phys. Chem.* **1993**, *97*, 6457−64.
(20) Frisch, M. J. Gaussian 92; Revision A; Trucks, G. W., Ed.; Gaussian Inc.: Pittsburgh, PA, 1992.
(21) Robinson, P. J.; Holbrook, K. A. *Unimolecular Reactions*; Wiley-Interscience: London, 1972.
(22) Vazquez, S. A.; Rios, M. A.; Carballeira, L. *J. Comput. Chem.* **1991**, *12*, 872−9.
(23) Inagaki, F.; Harada, I.; Shimanouchi. *J. Mol. Spectrosc.* **1973**, *46*, 381−96.
(24) Hirota, E. *J. Phys. Chem.* **1979**, *83*, 1457−65.
(25) Lien, M. H.; Hopkinson, A. C. *J. Comput. Chem.* **1985**, *6*, 274−81.
(26) Palke, W. E.; Kirtman, B. *J. Phys. Chem.* **1988**, *92*, 3046−8.
(27) Allinger, N. L.; Schmitz, L. R.; Motoc, I.; Bender, C.; Labanowski, J. K. *J. Am. Chem. Soc.* **1992**, *114*, 2880−3.
(28) *CRC Handbook of Chemistry and Physics*; 76th ed.; Lide, D. R., Ed.; CRC Press: Bota Raton, FL, 1995−1996.
(29) *CODATA Key Values for Thermodynamics*; Cox, J. D.; Wagman, D. D.; Medvedev, V. A., Eds.; Hemisphere Publishing Corp.: New York, 1989.
(30) McMillen, D. F.; Golden, D. M. *Ann. Rev. Phys. Chem.* **1982**, *33*, 493.
(31) Pople, J. A.; Luke, B. T.; Frisch, M. J. *J. Phys. Chem.* **1985**, *89*, 2198−203.
(32) Rossi, I.; Truhlar, D. G. *Chem. Phys. Lett.* **1995**, *234*, 64−70.
(33) Johston, H. S. *Gas Phase Reaction Rate Theory*; The Ronald Press: New York, 1966.
(34) Hirschfelder, J. O.; Curtiss, C. F.; Bird, R. B. *Molecular Theory of Gases and Liquids*; Wiley and Sons, Inc.: New York, 1954.